DOI: https://doi.org/10.54966/jreen.v28i1.1345

Journal of Renewable Energies

Revue des Energies Renouvelables

journal home page: https://revue.cder.dz/index.php/rer

Conference paper

Physico-chemical characterization of Al_2O_3/Ti6A4V type thermal barrier systems

Djamel Amari [a,*], **Khaoula Rahmouni** [b], **Nadia Saoula** [c], **Hafit Khireddine** [a], **Youcef Khelfaoui** [d]

[a] *Laboratoire de génie de l'environnement (LGE), Université de Bejaia, route de Targa Ouzamour, Bejaia, Algérie*

[b] *laboratoire des matériaux et composantes actives (LMCA), Institut des sciences et technologies appliquées (ISTA), Université de Oum El Bouaghi, 04000, Algérie*

[c] *Centre de Développement des Technologies Avancées (CDTA), Cité, 20 Août 1956, Baba Hassen, Alger, Algérie*

[d] *Laboratoire de mécanique, matériaux et énergétique (L2ME), Université de Bejaia, route de Targa Ouzamour, Bejaia, Algérie*

ARTICLE INFO

Article history:

Received November 25, 2024

Accepted January 29, 2025

Keywords:

Al_2O_3,
Ti6A4V,
Deposits,
Rugosité,
Crystallization,
Polarisation.

ABSTRACT

Al_2O_3 alumina deposits were deposited on Ti6A4V titanium alloy substrates by rf-PVD at different substrate polarizations 0V, -50V, -100V, and without polarization (wp). SEM images, at the surface of the deposits, showed a very good substrate coverage with a dense morphology. Quantitative EDS analysis of these deposits revealed the presence of the elements Al and O in these deposits. The mass percentage of these elements, at different polarizations of the substrate, varies between 51.72% and 56.19% for Al and between 43.80% and 48.27% for O. The images, revealed by AFM, showed well-spread deposits on the surface of the substrates with relatively uniform grooves. The values of the arithmetic roughness R_a, ranging from 3.45 to 4.75 nm, testify to the low crystallinity of these deposits and an appreciable density. The DRX of these deposits in 2θ mode showed a weak crystallization of the Al_2O_3 phase and characteristic peaks of the partially crystallized phases $Al_{0.3}Ti_{1.7}$, and $Ti_{0.7}V_{0.3}$, resulting from the interaction of the elements of the Ti6A4V substrate and those of the Al_2O_3 deposit.

1. INTRODUCTION

Understanding and predicting the behavior of matter are sources of progress and technological innovation. Today, materials, and in particular oxides, occupy a prominent place in many industrial sectors. Among these, aluminum oxide Al_2O_3, known as alumina, is a material with strong application

* *Corresponding author, E-mail address: djamel.amari@univ-bejaia.dz*

ISSN: 1112-2242 / EISSN: 2716-8247

potential due to its mechanical and electronic properties (Mir et al. 2021; Simoes, 2018; Cazajus et al. 2012). Aluminum oxide, in its amorphous state, is a good thermal and electrical insulator (Leyens & Peters, 2003). The microelectronics industry is interested in this material to develop new high-purity dielectrics at submicrometer scales (Leyens & Peters, 2003; Carter & Norton, 2007). It is thus seeking to precisely determine its thermal properties over a wide temperature range

Titanium alloys Ti6A4V are commonly used in extreme temperatures and environmental conditions. Ti6A4V is the most commonly used of all dual-phase titanium alloys, originally developed for the aerospace market and widely used in aerospace structural members (Uday et al. 2016). More recently, it has been used extensively in the oil and gas industry where a combination of high strength, high corrosion resistance, and low weight is essential (Uday et al. 2016). The exceptionally high hardness-ductility ratio with good fatigue resistance makes these alloys good candidates for the space industry (Cai et al. 2020; Lu et al. 2020).

Their mechanical properties, their resistance to creep at high temperatures, and their lightness make these alloys attractive materials for the aeronautics, space, and biomedical industries. Their use is already widespread in this sector, and many alloys have been developed to meet the specific needs of the aeronautics and space industries. In particular, turbine engine manufacturers, whose requirements for improving the efficiency and reducing the fuel consumption of their turbo machines mainly involve making engines lighter and increasing operating temperatures (Li et al. 2020). The density of the Ti6A4V alloy is half that of nickel alloys and stainless steel. They have a high strength-to-weight ratio (Cazajus et al. 2012). However, extending these alloys to higher engine temperature zones or increasing the operating temperature of the engines poses the problem of oxidation (Cai et al. 2020). While their oxidation kinetics remain acceptable up to temperatures of around 400°C, beyond 500°C (Cai et al. 2020), oxidation phenomena and their corollaries (scaling, embrittlement, etc.) can no longer be neglected (Cai et al. 2020; Lu et al. 2020; Lu et al. 2020; Li et al. 2020; Emadinia et al. 2020). The oxidation phenomenon is manifested by the rapid appearance of a TiO_2 type oxide layer followed by a significant loss of mass (Li et al. 2020).

This drawback, which has so far limited the use of these titanium alloys, is therefore becoming increasingly restrictive. The creation of alloys resistant to oxidation while retaining their mechanical properties does not seem likely to occur in the short term (Emadinia et al. 2020). This is why the solution of protective coatings is emerging as one of the simplest and most effective solutions (Marciolnilo et al. 2022; Travessa & Ferrante, 2002; Barrena et al. 2009).

The major worry of manufacturers is how to improve the resistance to surface oxidation of these alloys by reducing the diffusion of oxygen and nitrogen, and consequently, reduce their mass loss for operating temperatures above 600°C (Barrena et al. 2009; Bobzin et al. 2024; Xue et al. 2020; Silva et al. 2021a). The chemical and thermal stability of these alloys at high temperatures also constitutes a major challenge that seems far from being resolved (Bobzin et al. 2024; Xue et al. 2020; Silva et al. 2021a).

Direct deposition of an oxide layer resistant to oxygen and nitrogen diffusion is therefore the targeted strategy. Various materials have been applied, such as Si_3N_4, silica, or enamel layers (Barrena et al. 2009; Xue et al. 2020; Silva et al. 2021a) deposited by PVD or plasma spraying. Nitride-based ceramic multilayers have also been tested. Two types of structures have been tested, CrN/NbN and TiAlCrYN or TiAlYN/CrN. Applied to an α-TiAl titanium alloy, the TiAlCrYN/CrN system shows good resistance to isothermal oxidation between 750 and 1000°C by developing a surface oxide layer, which can even exceed the performance of the α-TiAl alloys tested in parallel under the same conditions (Silva et al. 2021b; Tang et al. 2000). However, prolonged oxidation periods induce the formation of defects in the nitrides that lead to oxidation of the substrate (Tang et al. 2000). However, the mechanical cohesion of the system also remains to be demonstrated.

Ion implantation has been performed, particularly on TiAl alloys. Silicon implantation does not improve resistance to cyclic oxidation. However, after annealing at 830°C for 10 h, the development of a mixed SiO_2-Al_2O_3 layer creates an effective oxide barrier (Taniguchi et al. 2001). The implantation conditions have little influence on the performance of these systems.

The application of metallic coatings that develop a protective oxide layer has also been tested. Coatings combining aluminum and transition metals (Al, Cr), (Al, Ti), or (Al, Ni) deposited by PVD are widely used. They are developed at low temperatures T< 200 °C and low pressure P = 0.5 Pa (Nicholls, 2003; Streiff, 1993; Park et al. 1997; Tang et al. 2000). The incorporation of transition metals makes it possible to increase the hardness of the aluminum layers and to modify the corrosion resistance properties.

In this work, we proposed to carry out deposits of Al_2O_3 type oxides (alumina) on a titanium alloy of the Ti6A4V type at different polarizations of the latter. The applied substrate polarizations are 0V, -50V, and -100V and without polarization (wp). The deposits carried out were carried out by PVD.

2. EXPERIMENTAL PROCEDURE

2.1 Deposition technique

The deposition of Al_2O_3 films on the Ti6A4V alloy is carried out by PVD-radio frequency (rf) at the Center for the Development of Advanced Techniques (CDTA) in Algiers. This device is designed and produced by the plasma and application team of the center. The deposition parameters used are illustrated in Table 1.

Before making these deposits on the Ti6A4V substrate, the latter was cut into (1×1) cm2 surface samples. To ensure a good surface condition of the substrate, polishing with SiC type abrasive papers, and with decreasing grain size, was carried out until its mirror state. The work of Amari et al. (2019) gives us more details on the operating conditions of PVD-rf deposits.

Table 1. Paramètres de dépôt de films Al_2O_3 sur le substrat Ti6A4V.

Generator	Target	Distance (cm)	Power (W)	Time (min)	Substrate	Gaz	flow (sccm)	Substrate polarization (V)
Radiofrequency (rf)	Al_2O_3	3	300	60	Ti6A4V	Ar	8	wp, 0V, -50, -100

2.2 Microscopy SEM-EDS and AFM characterization

Microstructures of deposits were observed on its surface using a scanning electronic microscope (SEM) from JEOL-DAC in high vacuum. Chemical composition was analyzed using an energy dispersive spectroscopy (EDS). The surface condition of the Al_2O_3 deposits and the roughness profile were carried out by AFM.

2.3 X-ray diffraction characterization

X-ray diffraction in 2θ Mode was performed on Al_2O_3/Ti6Al4V deposits by a Bruker AXS D8 Advance diffractometer of Al_2O_3/Ti6Al4V deposits at different substrate polarizations. The radiation wave used is of the monochromatic Cu Kα type with wavelength $\lambda_{(CuK\alpha)}$ = 1.54 Å for 2θ scan ranging from 20° to 120°.

2.4 AFM characterization

Surface images (1×1) µm² were obtained for Al_2O_3 deposits in contact mode, using an AFM, Asylum Research an Oxford Instruments Company MFP 3D, under ambient laboratory conditions. The pyramid tip radius used is 50 nm. A constant force of 0.032 N was applied.

3. RESULTS AND DISCUSSION

3.1 MEB-EDS microscopy

SEM images Figure 1, were obtained to identify the morphology of the Al_2O_3 deposits at different polarizations of the Ti6A4V substrate (wp, 0V, -50V, and -100V). The micrographs show an identical morphology of the Al_2O_3 deposits for different polarizations of the Ti6A4V substrate. The polarization of the substrate does not seem to have a significant influence on the morphology of the Al_2O_3 deposits (Wang et al. 2021). It should be noted, however, that the Ti6A4V substrate has an acceptable coverage of the Al_2O_3 deposit, and this is for the different polarizations of the substrate. The micrographs also show a relatively acceptable density of the Al_2O_3 deposit with porosities characteristic of PVD deposits (Damani & Makroczy, 2000). The furrows observed on the micrographs are probably due to polishing.

Quantitative EDS analysis Figure 2, performed on the Ti6A4V substrate without deposition, indicates a mass percentage (wt)% of the elements Ti, Al, and V of 85.14 (wt)%, 8.74 (wt)% and 6.11 (wt)%, respectively. On the other hand, the corresponding atomic percentage (at)% of these elements Ti, Al, and V are 80.02 (at)%, 14.57 (at)%, and 5.40 (at)%, respectively.

Regarding the quantitative analysis of Al_2O_3 deposits at different substrate polarizations Figure 3, these were deposited on glass slides because the substrate also contains aluminum. The results of the analysis are shown in Table 2 below.

Table 2. Quantitative EDS analysis of Al_2O_3 deposits at different polarizations of Ti6A4V substrate.

Polarisation	0V		-50V		-100V	
Elements present in the Al_2O_3 deposit (wt %)	Al	O	Al	O	Al	O
	55.89	44.10	51.72	48.27	56.19	43.80

The results in Table 2, indicate the presence of Al and O elements in the Al_2O_3 deposits, and this at different polarizations of the Ti6A4V substrate. For the 0V polarization of the substrate, the presence of Al in the deposit is 55.89 (wt)% and 44.10 (wt)% of O. On the other hand, for the -50V polarization of the substrate, the aluminum present in the Al_2O_3 deposit is 51.72 (wt)% for 48.27 (wt)% of O. Finally, for the -100V polarization, the presence of both Al and O elements in the Al_2O_3 deposit is 56.19 (wt)% and 43.80 (wt)%, respectively.

3.2 X-ray diffraction

X-ray diffraction in 2θ mode of Al_2O_3/Ti6Al4V deposits at different substrate polarizations reveals identical spectra. The identification of the phases formed in the Al_2O_3 deposit and at different substrate polarizations Ti6A4V shows the formation of the phases $Al_{0.3}Ti_{1.7}$ (ICDD: 01-077-6855), $Ti_{0.7}V_{0.3}$ (ICDD: 01-081-9817) and Al_2O_3 (ICDD: 01-074-7230) (Schoderböck, 2023). The elements Ti and V come from the substrate. We note that the spectrum of samples polarized at -100V, presents a peak with relatively lower intensity than those of samples polarized at -50V, 0V, and wp.

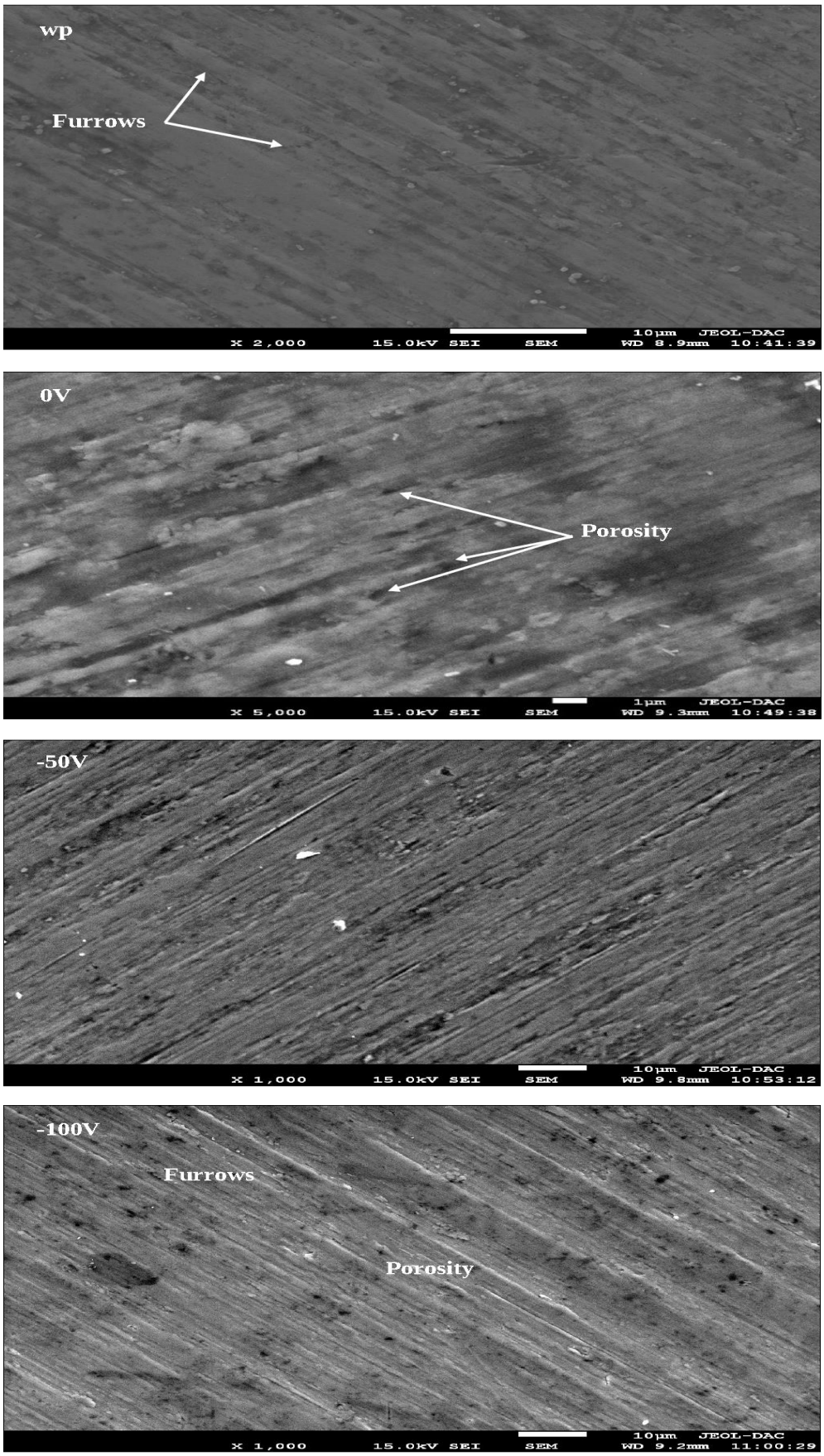

Fig 1. SEM micrography of Al_2O_3 deposits at different polarizations on Ti6A4V substrate.

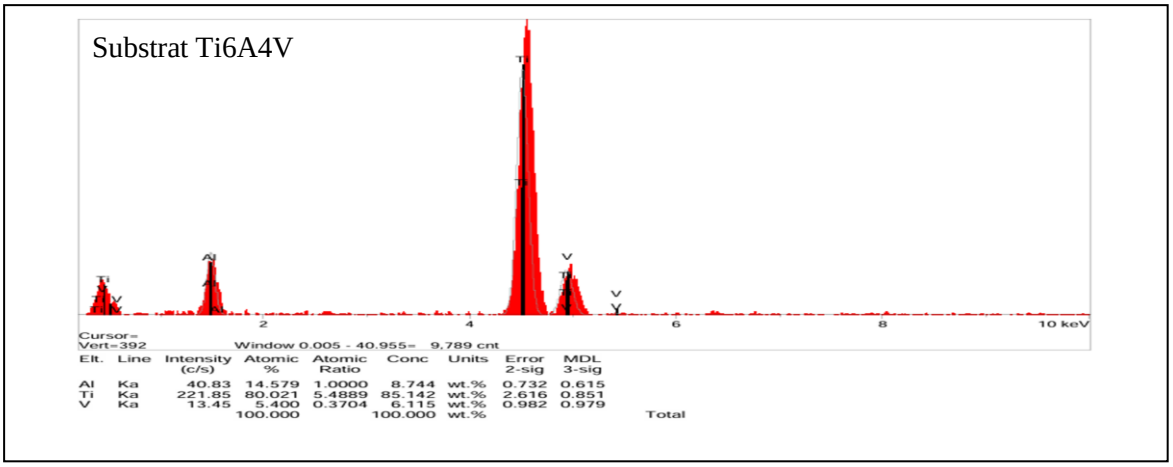

Fig 2. Quantitative EDS analysis of Ti6A4V substrate without deposition.

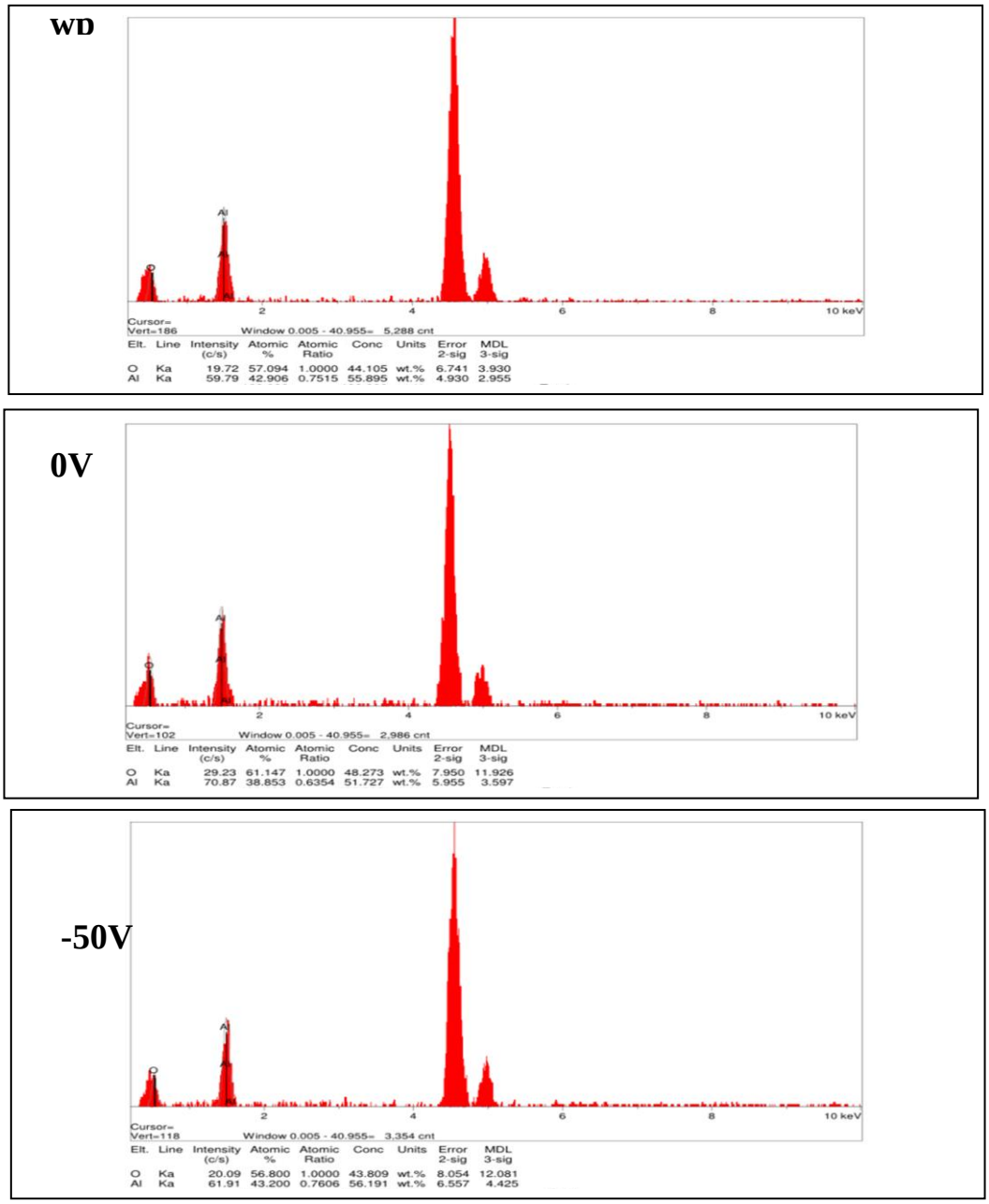

Fig 3. Quantitative EDS analysis of Al_2O_3 deposits at different substrate polarizations.

This phenomenon can be attributed to the partial crystallization of the phases (Schoderböck, 2023). 120°, we also note the presence of two phases $Al_{0.3}Ti_{1.7}$ and Al_2O_3 but at low intensity which indicates the partial crystallization of the latter. For the diffraction peaks at 80° < θ 2< 120° where we record the majority presence of the $Al_{0.3}Ti_{1.7}$ phases. Likewise, for the diffraction peaks between 50°< θ 2< 80°, the Al_2O_3 phase is present at low intensity for a diffraction angle 2θ ~ 57° and 75°.

The appearance of the low intensity diffraction peaks, representing the Al_2O_3 phase are less sharp compared to the peaks of the crystallized phases. This lets us say that the Al_2O_3 deposits made on the Ti6A4V substrate are of amorphous structures (Schoderböck, 2023).

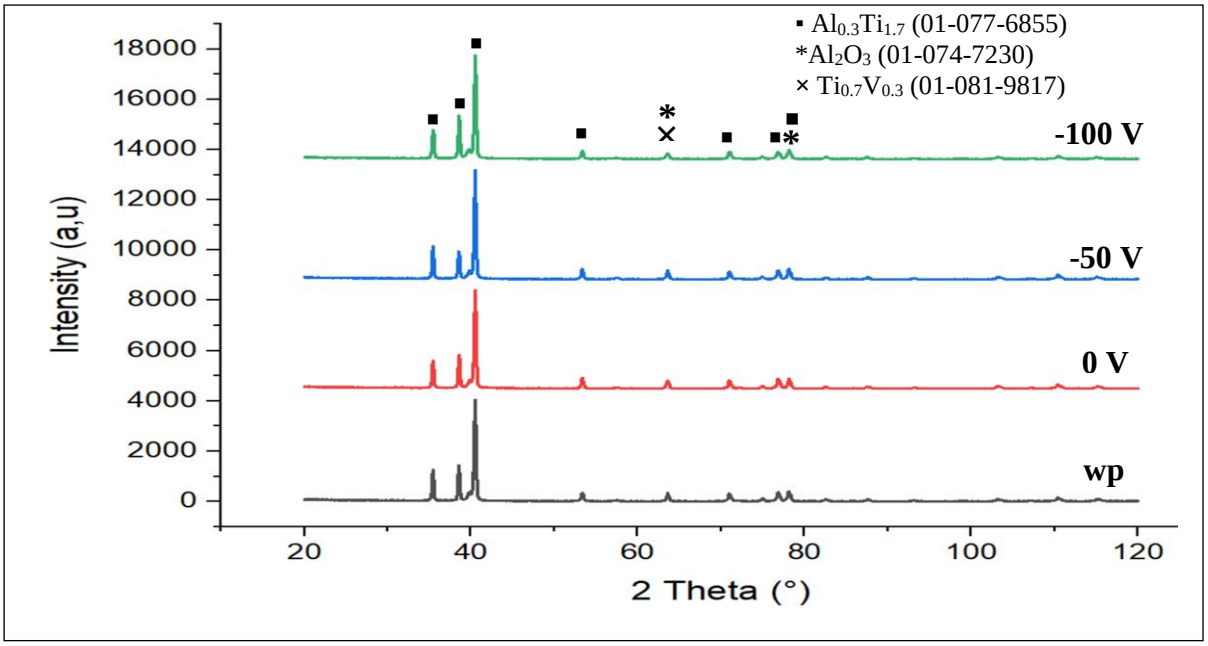

Fig 4. X-ray diffraction of Al_2O_3/Ti6A4V deposits at different substrate polarizations.

3.3 The crystallite size of phases

Calculation of the mean crystallite size (MCS) of the phases as a function of substrate polarization was determined by the following formula (Soo-Wohn et al. 2013).

$$MCS = \frac{K.\lambda}{FWHM.cos\theta} \quad (1)$$

Where K is a constant (k = 0.9), λ is the wavelength used (λ = 0.054 nm), FWHM is the width at half-height of the most intense peak in the spectrum of each deposit and θ is the diffraction angle of the most intense peak. Table 3, below summarizes these calculations.

Table 3. Calculation of the average size of MCS crystallites.

Phases	Position (2θ°) of the most intense peak	FWHM (2θ°)	MCS (nm)
Al_2O_3	40.46	0.2424	0.263
$Al_{0.3}Ti_{1.7}$	40.46	0.2423	0.263
$Ti_{0.7}V_{0.3}$	39.96	0.9001	0.070

Based on calculations of the mean crystallite size of the phases at the most intense peak, we note that the mean crystallite size in the majority of Al_2O_3 and $Al_{0.3}Ti_{1.7}$ phases is the same, equal to 0.263 nm. In contrast, the $Ti_{0.7}V_{0.3}$ minority phase shows a very small crystallite size of 0.070 nm.

From this observation, we can deduce that the microstructure of the deposits is composed of very fine dense grains.

3.4 AFM microscopy

Figure 4, represents the 3D topography and roughness profile for each Al_2O_3 deposit as a function of the polarization of the Ti6A4V substrate. These micrographs are determined by the contact mode and for a scanned surface of (1 x 1) μm^2. The results of the arithmetic roughness R_a of these deposits give values between 3.45 and 4.75 nm. We note that the Al_2O_3 deposits have a relatively uniform surface state, with regular geometry and with small grains. The low roughness observed for these deposits lets us say that they are dense and have a low stress concentration. This low surface stress concentration plays a key role in determining the corrosion resistance of these deposits.

We note, however, that the arithmetic roughness R_a of the Al_2O_3 deposits increases as a function of the negative polarization of the Ti6A4V substrate. The favorable role of negative substrate bias on the texture of Al_2O_3 deposits is explained by the increase in kinetic energy and positive ion flux in the plasma with the negative bias voltage (Derniaux, 2007; Dalmas, 2005). The energy provided by these ions increases the mobility of species on the surface of the film and promotes the rearrangement of adatoms according to the densest planes of the Al_2O_3 structure (Lee & Lee, 1997). A moderate increase in substrate bias improves the texture of the deposits (Lee & Lee, 1997). For a larger negative bias, the crystallographic orientation of the deposit layers deteriorates (Lee et al. 1994). These results are in agreement with the study conducted by Lee et al. (1994) concerning the influence of substrate bias on the preferential orientation of AlN layers developed by rf- magnetron sputtering on silicon substrates. These studies suggest that the significant increase in negative substrate bias also increases the roughness of Al_2O_3 deposits.

CONCLUSION

This work of physicochemical characterization of Al_2O_3/Ti6A4V films, deposited by PVD-rf at different polarizations of the substrate, allowed us to conclude the following bridges:

- The morphology at the SEM of the Al_2O_3 deposits is identical, fine, dense, and well spread on the Ti6A4V substrate, and this is for the different polarizations. The porosities observed on the deposits are typical of PVD deposits;
- The polarization of the Ti6A4V substrate seems not to have any influence on the morphology of the deposits;
- The DRX indicates the presence of the crystallized phases $Al_{0.3}Ti_{1.7}$ and $Ti_{0.7}V_{0.3}$ of the substrate. On the other hand, the Al_2O_3 phase, at low intensity, is amorphous;
- The crystallites of the deposits are fine with a dimension of 0.26 nm, testifying to the density of these deposits;
- AFM indicates a uniform and regular morphology of the Al_2O_3 deposits, well spread on the Ti6A4V substrate. A relatively uniform roughness profile indicates a roughness Ra varying between 3.45 and 4.75 nm. This roughness increases as a function of increasing the negative polarization of the Ti6A4V substrate.

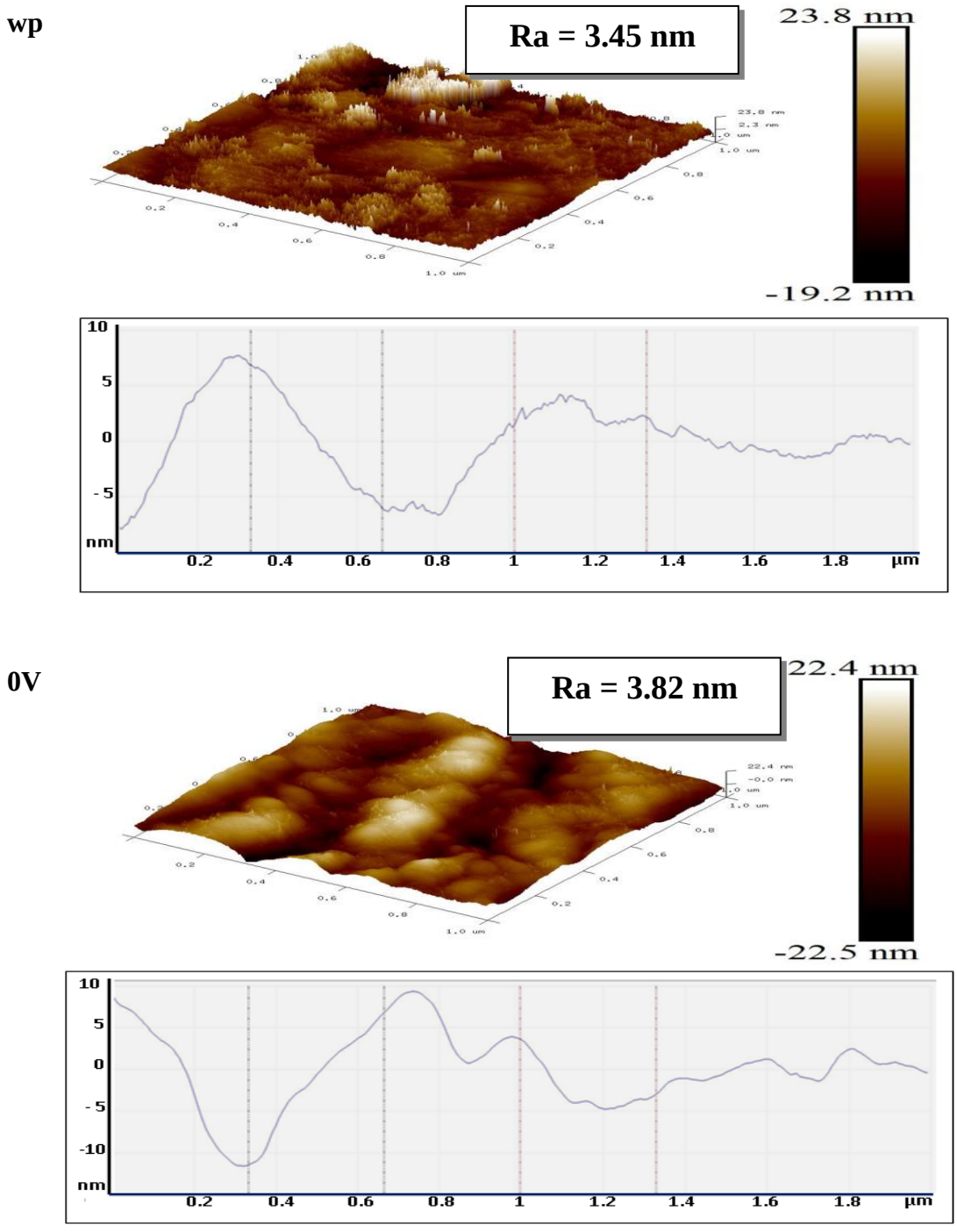

Figure 4. 3D topography and roughness profile for each Al2O3 deposit as a function of the polarization of the Ti6A4V substrate

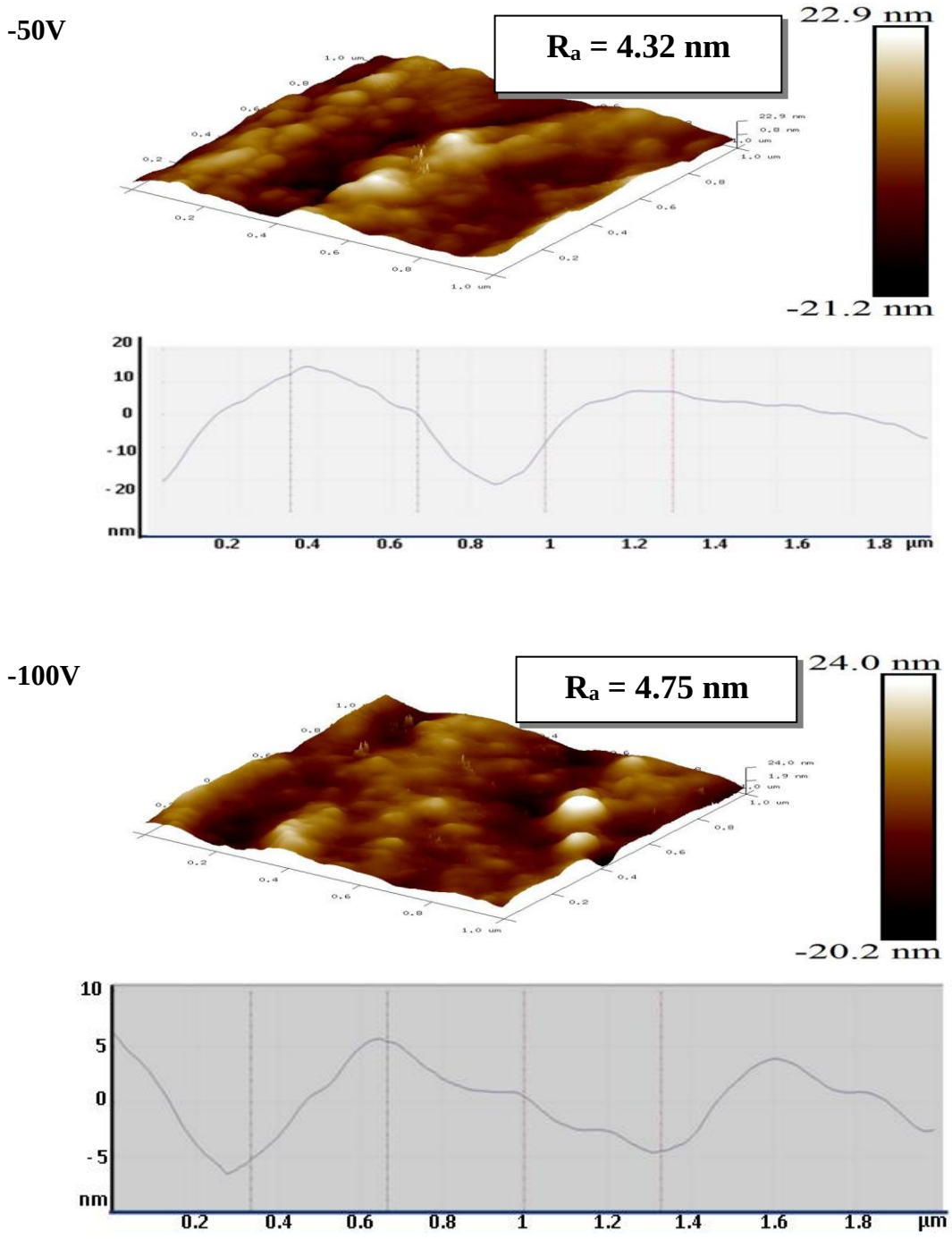

Figure 4. 3D topography and roughness profile for each Al2O3 deposit as a function of the polarization of the Ti6A4V substrate *(Continued)*

ACKNOWLEDGEMENTS

The authors would like to thank the Advanced Technology Development Center (CDTA) in Algiers, in particular Prof. N Saoula, research director at the center, for the realization of the Al_2O_3/Ti6A4V deposits by PVD-rf. We would also like to thank Dr. Rahmouni from the Institute of Applied Sciences and Technology (ISTA) in Oum el Baouaghi for his contribution to the realization of the SEM micrographs.

NOMENCLATURE

Al_2O_3	alumina	λ	wavelength [Å]
Ti6A4V	Titanium alloys	Cu-Kα	type of cathode used
PVD-rf	physical vapor deposition radio frequency	θ	diffraction angle [°]
		(wt)	masse percentage
SEM	scanning electron microscopy	(wa)	atomic percentage
EDS	energy dispersive spectroscopy	ICDD	International Center for diffraction data base
AFM	atomic force microscopy		
DRX	X-ray diffraction	MCS	mean crystallites size
P	Pression [Pa]	FWHM	with at half height of the most intense peak [rad]
wp	Without polarization		
T	Temperature [°C]	R_a	arithmetic roughness [nm]
Sccm	standard cubic centimeters per minute		

REFERENCES

Amari D, Khireddine H, Khelfaoui Y, Saoula N. (2019). Adhesion and Corrosion of Ti, TiN and TiCrN Films Deposits on AISI 316L in SBF Solution, Def and Diff Forum, ISSN: 1662-9507, Vol. 397, pp 39-50.

Barrena M.I, Matesanz L, de Salazar J.M.G. (2009). Al_2O_3/Ti6Al4V diffusion bonding joints using Ag-Cu interlayer. Mater. Charact. 60, 1263–1267.

Bobzin K, Kalscheuer C, Mobius M P ,Hassanzadegan Aghdam P. (2024). Thermal stability of thick α- and γ-Al2O3 coatings deposited by high-speed PVD Surf & Coat Tech 477. 130411.

Cai X Q, Wang D P, Wang Y, Yang Z W.(2020). Microstructural evolution and mechanical properties of TiB2-TiC-SiC ceramics joint brazed using Ti-Ni composite foils. J. Eur. Ceram. Soc. 40, 3380 –3390.

Carter CB, Norton M.G. (2007). Ceramic Materials; Springer: New York, NY, USA, ISBN 978-0-387-46270 -7.

Cazajus V, Seguy S, Welemane H (2012). Karama, M. Residual stresses in a ceramic-metal composite. Appl. Mech. Mater, 146, 185 – 196.

Damani R J, Makroczy P. (2000). Heat Treatment Induced Phase and Microstructural Development in Bulk Plasma Sprayed Alumina, *J. Europ. Ceram. Soc.*, vol. 20, pp. 867-888.

Delmas M. (2005). Revêtements aluminium-platine obtenus par dépôt chimique en phase vapeur pour la protection de l'alliage Ti6342 contre l'oxydation à des températures inférieures à 600°C, thèse de doctorat, institut polytechnique de toulouse.

Derniaux E, (2007). Etude de structures NiCoCrAlY/Al2O3/TiO/Pt/AlN déposées par pulvérisation cathodique sur superalliage base Ni pour capteurs de pression haute température, thèse de doctorat, univ. Caen/basse-normandie.

Emadinia O, Guedes A, Tavares C J, Simões S. (2020). Joining Alumina to Titanium Alloys Using Ag-Cu Sputter-Coated Ti Brazing Filler. Materials. 13, 4802.

Lee H C, Lee J Y, Ahn H J. (1994). Effect of the substrate bias voltage on the crystallographic orientation of reactively sputtered AlN thin films. Thin Solid Films 251, pp. 136-140.

Lee H C, Lee J Y. (1997). Effect of negative bias voltage on the microstructures of AlN thin films fabricated by reactive r.f. magnetron sputtering, Mater. Sci.: Mater. Electron 8, pp. 385-390.

Leyens C, Peters M. (2003). Titanium and Titanium Alloys; Wiley: Hoboken, NJ, USA, ISBN 9783527305346.

Li C, Zhang K, Mao X, Si X, Lan B, Liu Z G, Huang Y, Qi J, Feng J, Cao J. (2020). Microstructure and mechanical properties of the AlON / Ti6Al4V active element brazing joint. Mater. Sci. Eng. A. 793, 139859.

Lu Y, Zhu M., Zhang Q, Hu T, Wang J, Zheng, K. (2020). Microstructure evolution and bonding strength of the Al_2O_3/Al_2O_3 interface brazed via Ni-Ti intermetallic phases. J. Eur. Ceram. Soc. 40, 1496–1504.

Marcionilo S J r, Ramos A S, Teresa M V, Simões S. (2022). Joining of Ti6Al4V to Al_2O_3 Using Nanomultilayers, Nanomaterials, 12, 706. https://doi.org/10.3390/ nano12040706.

Mir F A, Khan, N Z, Parvez S. (2021). Recent advances and developments in joining ceramics to metals. Mater. Today Proc., 46, 6570 – 6575.

Nicholls J R. (2003). Advances in Coating Design for High-Performance Gas Turbines, *MRS Bulletin*, vol. September, pp. 659-670.

Park J Y, Park S W, Lee H N, Oh M H, Wee D M. (1997). $(Al, Cr)_3Ti$-based two phase intermetallic compounds-II. Application to coating materials on TiAl, *Scrip. Mater.*, vol. 36, pp. 801-806.

Schoderböck P. (2023). On the relationship between texture characteristics and residual stress levels: An X-ray diffraction study on α-Al_2O_3 hard coatings**.** Thin Sol Films. V.777, 139893.

Silva M, Ramos A S, Vieira M.T, Simões S. (2021a). Diffusion Bonding of Ti6Al4V to Al_2O_3 Using Ni/Ti Reactive Multilayers. Metals. 11, 655.

Silva M, Ramos A.S, Simões S. (2021b). Joining Ti6Al4V to alumina by diffusion bonding using titanium interlayers. Metals. 11, 1728.

Simões S. (2018). Recent Progress in the Joining of Titanium Alloys to Ceramics. Metals, 8, 876.

Soo-Wohn L, Paraguay-Delgado F, Arizabalo R D , Gómez R_Rodríguez-González V. (2013). Understanding the photophysical and surface properties of TiO_2–Al_2O_3 nanocomposites. Mat Lett. V. 107, P 10-13.

Streiff R. (1993). Protection of materials by advanced high temperature coatings," *J. Phys. IV*, vol. 3, pp. 17- 41.

Tang Z, Wang F, Wu W. (2000). Effetcs of Al_2O_3 and enamel coatings on 900°C oxidation and hot corrosion behavior of Gamma-TiAl," *Mat. Sci. Eng. A*, vol. 276, pp. 70-75.

Taniguchi S, Shibata T, Yamada T, Liu X, Zou S. (2001). *ISIJ Int.*, vol. 33, pp. 869, 1993.

Travessa D, Ferrante M. (2002). The Al_2O_3-titanium adhesion in the view of the diffusion bonding process. J. Mater. Sci. 37, 4385–4390.

Uday M B, Ahmad F M.N, Noor AM., Rajoo S. (2016). Current Issues and Problems in the Joining of Ceramic to Metal. In Joining Technologies; Ishak, M., Ed.; InTech: Rijeka, Croatia, Chapter 8.

Wang R, Dong X, Wang K, Sun X, Fan Z, Duan W, Byung-Guk J M. (2021). Polarization effect on hole evolution and periodic microstructures in femtosecond laser drilling of thermal barrier coated superalloy, App Surf Sci, Vo 537, 148001.

Xue H, Wei X, Guo W, Zhang X. (2020). Bonding mechanism study of active Ti element and _-Al_2O_3 by using first-principle calculation. J. Alloys Compd. 820, 153070.